ACS Synthetic Biology

Article

Tuning vector stability and integration frequency elevates functional GPCR production and homogeneity in Saccharomyces cerevisiae

Justin Yoo, and Michelle A O'Malley

ACS Synth. Biol., **Just Accepted Manuscript** • DOI: 10.1021/acssynbio.8b00036 • Publication Date (Web): 05 Jun 2018

ACS Publications

is published by the American Chemical Society. 1155 Sixteenth Street N.W., Washington, DC 20036

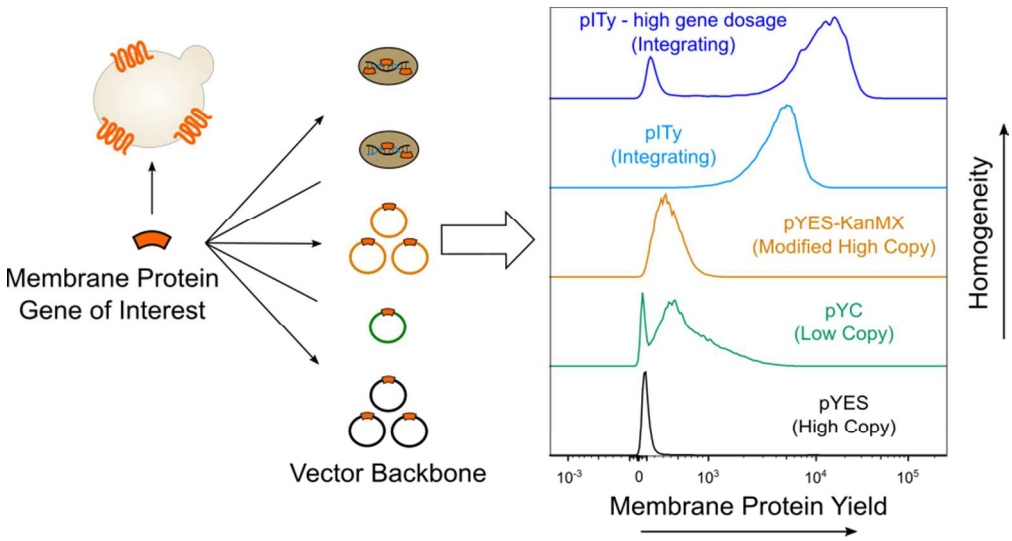

342x181mm (72 x 72 DPI)

Tuning vector stability and integration frequency elevates functional GPCR production and homogeneity in *Saccharomyces cerevisiae*

Justin I. Yoo[1], Michelle A. O'Malley*[1]

[1]Department of Chemical Engineering, University of California Santa Barbara, Santa Barbara, CA 93106, United States

*E-mail: momalley@ucsb.edu

Abstract

Membrane proteins play a valuable role in biotechnology, yet the difficulty of producing high yields of functional membrane protein limits their use in synthetic biology. The practical application of G protein-coupled receptors in whole cell biosensors, for example, is restricted to those that are functionally produced at the cell surface in the chosen host, limiting the range of detectable molecules. Here, we present a facile approach to significantly improve the yield and homogeneity of functional membrane proteins in *Saccharomyces cerevisiae* by altering only the choice of expression vector. Expression of a model GPCR, the human adenosine A_2a receptor, from commonly used centromeric and episomal vectors leads to low yields and cellular heterogeneity due to plasmid loss in 20 – 90% of the cell population. In contrast, homogenous production of GPCR is attained using a multi-site integrating vector or a novel, modified high copy vector that does not require genomic integration or addition of any selection agents. Finally, we introduce a FACS-based screen, which enables rapid isolation of cells with 4- to 15-fold increases in gene dosage and up to a 9-fold increase in functional protein yield without loss of homogeneity compared to a strain isolated through conventional, low-throughput methods. These results can be extended to improve the cellular homogeneity and yield of other membrane proteins, expanding the repertoire of useful receptors for synthetic biology applications.

Keywords: Membrane protein; GPCR; vector; yeast; homogeneity; biosensor

Membrane proteins have great value in biotechnology such as in microbial cell factories[1] and as natural biosensors. However, these proteins are notoriously difficult to produce at high yields in functional form using heterologous hosts such as *Saccharomyces cerevisiae*, often precluding their characterization and use in downstream applications[2]. For example, G protein-coupled receptors (GPCRs) are promising candidates to drive whole cell biosensors[3] to address the need for low-cost, high-throughput screening of valuable chemicals[4]. To date, however, GPCR-based yeast biosensors have been constructed[5–9] without optimization of the cellular homogeneity or yield of functional protein. Both of these factors critically impact the sensitivity of GPCR signaling[10], as well as a cellular biosensor's dynamic range. Additionally, although GPCRs are currently targeted by ~34% of FDA-approved drugs[11], low yields of thermostable, functional protein often hampers the generation of high quality crystal structures to inform structure-based drug design[12]. Approaches to improve membrane protein yield[13] are generally cumbersome and can affect the protein's structure, potentially obscuring its true quaternary structure.

Of all parameters that drive membrane protein expression in recombinant systems, the choice of expression vector is easy to modify, but is almost always chosen empirically. In eukaryotic systems like yeast, plasmids can directly affect both protein yield and gene product heterogeneity through copy number and mitotic stability[14,15]. While the effects of vector choice on protein yields and cellular homogeneity have been extensively investigated for soluble and secreted proteins, by comparison the expression of membrane proteins in *S. cerevisiae* has been carried out *ad hoc* for decades. For example, heterologous membrane protein overexpression in *S. cerevisiae* is most often performed using episomal vectors as evidenced by their exclusive use, at present, in producing high resolution crystal structures (**Table S2**)[16–30]. While high copy, autonomously replicating plasmids may be useful for soluble proteins, this chassis may not be suitable for many membrane proteins due to the metabolic burden associated with saturating the yeast secretory pathway[31], which is

particularly problematic for proteins of human origin. Centromeric vectors are thought to afford a compromise between stability and copy number, providing stably maintained plasmids at low copies[32]. However, plasmid loss has also been reported upon use of this system[33], which limits protein yields. Despite the variable phenotypes resulting from use of these plasmids, their use is preferable over more stable integrating vectors for applications where genomic integration is cumbersome, such as in protein engineering.

In this work, we demonstrate that the vector backbone can be used as a single parameter to improve the yield and homogeneity of a model GPCR, the human adenosine A_2a receptor (hA_2aR). While expression of *A_2aR* from commercial high and low copy vectors results in significant phenotypic heterogeneity, the use a modified high copy vector leads to a homogeneous cell population without genomic integration or addition of a selection agent. Gene expression from a multi-site integrating vector results in the greatest yield of functional A_2aR while maintaining high homogeneity. Further, we developed a rapid screening protocol to isolate yeast strains with high, tunable yields of functional hA_2aR without loss of homogeneity through increasing gene dosage of the integrating vector.

Results and Discussion

Common yeast vectors produce a range of membrane protein yields and homogeneity

To determine which vector system would result in the greatest yield and homogeneity of hA_2aR production, a galactose-inducible hA_2aR-GFP-His_{10} (A_2aGH) gene cassette was subcloned into three yeast vectors with varying reported copy numbers and mitotic stabilities (**Table 1**)[32,34,35]. C-terminal GFP tags have been used previously to monitor membrane protein production in *S. cerevisiae*[36] and provides a proxy measurement to assess total protein yields. Clear differences in

both cellular mean fluorescence intensity (MFI) and homogeneity were evident upon gene expression and analysis by flow cytometry (**Figure 1**).

Table 1: Characteristics of yeast vectors used in this study

vector	vector class	anticipated copy number ($cell^{-1}$)[a]	mitotic stability
pITy	Integrating	1 - 30	+++
pYC2/CT	Centromeric	1 - 2	++
pYES2	Episomal	10 - 40	+

[a] 32, 34, 35

Despite having the greatest maximal anticipated copy number, the high copy backbone (pYES) yields a 4.9-fold increase in cellular MFI over background autofluorescence (indicative of A_2aGH production), the lowest value among the vectors tested in this study (**Figure 1A**). This result is due to the large fraction (91%) of cells displaying fluorescence intensities comparable to autofluorescence (**Figure 1B and S1A**). Flow cytometry has been used previously to associate basal fluorescence intensities with plasmid loss in cells producing a GFP-tagged protein[37]; thus, we hypothesized that the significant fraction of cells exhibiting background MFI emerged due to plasmid loss and preferential propagation of plasmid-free cells. High copy vectors are known to exhibit the lowest mitotic stability among the vector classes tested in this work. Indeed, Wittrup *et al.* observed similarly extreme observations of mitotic instability upon production of secreted proteins in *S. cerevisiae*, wherein yields of multiple secreted proteins were greater using a centromeric vector compared to an episomal vector[31,38]. Although the authors did not quantify plasmid copy numbers, they attributed the unexpected results at least in part to episomal plasmid loss due to the metabolic burden associated with saturating the yeast secretory pathway[38].

To rule out artefactual plasmid loss due to mutations in the plasmid backbone, regulatory regions of the vector were sequenced and found to contain no mutations in the P_{URA3}, *URA3*, or 2μ ORI domains. Thus, we sought to increase the high copy vector's mitotic stability to reduce plasmid loss. Accordingly, we constructed a novel vector (pYES-KanMX) through introduction of *NEO*, a strong selection marker conferring resistance to G418, into the high copy vector backbone. Yeast expressing *A_2aGH* from this vector display a 5.3-fold increase in MFI over background, which is comparable to the value obtained using the unmodified vector (**Figure 1A**). However, strains harboring the modified vector exhibit a homogenous cell population even in the absence of the corresponding antibiotic (**Figure 1B and S1B**). In fact, cellular MFI was slightly reduced in the presence of G418 (**Figure S2**). Interestingly, this strain displays greater homogeneity compared to a strain expressing *A_2aGH* from a low copy centromeric vector. Although centromeric vectors are often used due to their high mitotic stability and concomitant homogeneity of protein production, expression of *A_2aGH* from a centromeric vector (pYC) produces a significant subpopulation of cells (~18%) exhibiting background levels of fluorescence intensity (**Figure 1B and S1C**). Further, the distribution of the fluorescent subpopulation in this strain is broader than that of the homogenous pYES-KanMX-harboring strain.

In contrast to the commercial, non-integrating plasmids, use of a multi-site yeast integrating vector (pITy) results in homogenous A_2aGH production contributing to 62-, 7-, and 13-fold increases in cellular MFI compared to background and strains expressing *A_2aGH* from centromeric and episomal vectors, respectively (**Figure 1 and S1D**). This choice of vector diverges from the current paradigm for membrane protein overexpression in *S. cerevisiae*, which largely relies on high copy plasmids. For example, screens to assess membrane protein production in *S. cerevisiae* commonly utilize episomal vectors[36,39–41], which may lead to low yields due to the choice of vector as opposed to inherent limitations of the protein or host. Our results suggest that screening membrane proteins

with these two common yeast vectors may lead to the erroneous conclusion that the host or protein, itself, must be modified to optimize yields or homogeneity. In contrast, the use of integrating vectors has been the established route for membrane protein production in the yeast *Pichia pastoris*, which has served as a popular host for membrane protein structural biology[42].

Integrating and modified high-copy vectors preclude plasmid loss associated with commercial, non-integrating plasmids

To test our hypothesis that cellular heterogeneity is a result of plasmid loss, the extent of plasmid loss was quantified in strains harboring non-integrating vectors prior to and during *A_2aGH* expression. Approximation of plasmid loss was performed by determining colony forming units (CFU) using permissive and selective media. In agreement with observations made with flow cytometry, strains harboring pYC A_2aGH and pYES A_2aGH exhibit a reduction in plasmid retention from 86% to 62%, and 16% to 1%, respectively, upon induction of gene expression (**Figure 2**). In contrast, strains containing pYES-KanMX A_2aGH show statistically insignificant plasmid loss before and during *A_2aGH* expression (**Figure 2**). Surprisingly, strains harboring pYES A_2aGH display high rates of plasmid loss prior to induction of gene expression. Analysis of strains using flow cytometry did not reveal leaky expression of *A_2aGH* prior to induction of gene expression.

Determination of vector copy numbers through quantitative PCR further corroborates our observations of plasmid loss in strains carrying high copy vectors (**Figure 3**). The relative copy number of the centromeric vector is 2.5-fold greater than that of the high copy vector, further evidencing high rates of pYES A_2aGH plasmid loss (**Figure 3**). It should be noted that the copy number is an average of the entire cellular population, thus the measured deviations from average do not reflect the heterogeneities observed in single cell analyses such as flow cytometry. Surprisingly, the pYES-KanMX copy number is 23-fold greater than that of the episomal vector,

indicating that the low A_2aGH yield associated with pYES-KanMX is not due to a decrease in plasmid copy number below a stable threshold quantity. Instead, we speculate that the expression of *NEO* and concomitant utilization of transcriptional and translational machinery introduces a bottleneck to A_2aGH production reducing cellular stress and mitotic instability. Since *NEO* encodes for a soluble, cytoplasmic class of proteins[43], its production is not expected to contribute to saturation of the yeast secretory pathway. The narrow fluorescence distribution associated with pYES-KanMX A_2aGH (**Figures 1B and S1B**) may also be a result of an artificial translational bottleneck as this phenomenon has previously been shown to reduce phenotypic noise associated with gene expression[44].

Concurrent *NEO* expression improves homogeneity of Ste2p GPCR production in the pYES-KanMX backbone compared to an unmodified episomal vector

Next, we sought to investigate the effects of *NEO* expression on A_2aGH production and investigate the applicability of this strategy to other high copy vector backbones. Therefore, we constructed a vector (tTA-KanMX A_2aGH) containing a galactose-inducible *A_2aGH* gene cassette as well as a tTA-KanMX cassette, which regulates *NEO* expression through the tetracycline-responsive tetR-VP16 transactivator (**Figure S2A**). In the absence of tetracycline, or a structural analog (i.e. doxycycline), tetR-VP16 binds to tetracycline operator (tetO) domains upstream of a minimal P_{CYC1} promoter and the *NEO* coding sequence inducing gene expression (**Figure S2B**). As doxycycline is added to the culture exogenously, tetR-VP16 unbinds the tetO domains in a dose-dependent manner[45]. If the transcription or translation of NEO contributes to increased cellular homogeneity of A_2aGH production, then we expect an inverse relationship between cellular homogeneity and exogenous doxycycline concentration. However, as doxycycline is added to the culture medium both total protein yield and cellular homogeneity increase in a sigmoidal fashion (**Figure S3**). Importantly, the reduced fluorescence intensities and homogeneities exhibited by cells exposed to low doxycycline

concentrations are not a result of plasmid loss (**Figure S4**). Instead, the reduced fluorescence intensities may be a result of transcriptional and/or translational bottlenecks associated with *NEO* expression as proposed previously. The discrepancy between the tTA KanMX A_2aGH and pYES-KanMX A_2aGH systems may be a result of switching to a different episomal backbone. Further investigations are required to elucidate the mechanism of action in both the tTA-KanMX and pYES-KanMX systems.

Although the tTA-KanMX system did not recapitulate the cellular homogeneity observed using pYES-KanMX A_2aGH, we sought to reproduce this behavior for another GPCR with the pYES-KanMX backbone. We chose the *S. cerevisiae* Ste2p GPCR since this protein has been the subject of several protein engineering[46–48] and synthetic biology[49] investigations; thus, information regarding Ste2p yield and homogeneity is valuable for optimizing similar studies in the future. Accordingly, *Ste2p-GH* expression from the pYC, pYES-KanMX, and YEp351 backbones was investigated using flow cytometry. The YEp351 backbone is another commonly used episomal backbone and provides a second reference for high copy gene expression. Flow cytometric analysis reveals anticipated relative yields and homogeneities for *Ste2p-GH* expression from the centromeric and episomal backbones. Cells harboring pYC Ste2p-GH and YEp351 Ste2p-GH exhibit 14.2- and 103.9-fold MFI over background, respectively (**Table S3**). While 88.2% and 79.3% of cells harboring the centromeric and episomal vectors, respectively, exhibit MFI over background the distributions of these subpopulations are distinct (**Figure S5**). The fluorescent subpopulation of cells harboring pYC Ste2p-GH (i.e. those within the gate) comprises a unimodal distribution with a robust coefficient of variance (RCV) of 94.2. In contrast, the fluorescent subpopulation of cells harboring YEp351 Ste2p-GH comprise a bimodal distribution with a RCV of 360.3. Cells expressing *Ste2p-GH* from pYES-KanMX exhibit 50.8-fold MFI over background, a 3.6-fold increase and 2,0-fold decrease relative to the pYC and YEp351 backbones, respectively (**Table S3**). Interestingly, these cells

maintain a unimodal fluorescent subpopulation with a RCV of 149.2, a 1.6-fold increase and 2.4-fold decrease relative to pYC and YEp351, respectively (**Figure S5** and **Table S3**). These results corroborate the utility of the pYES-KanMX backbone in improving cellular homogeneity relative to commonly used high copy vectors such as YEp351. In this case, the cellular homogeneity was slightly decreased compared to the centromeric system; however, the total membrane protein yield was improved by a greater margin. If *NEO* expression is responsible for the phenotypic changes observed in the pYES-KanMX system, it may be possible to improve the homogeneity of Ste2p production by altering *NEO* expression levels (e.g. through changing the promoter).

FACS screen enables rapid isolation of strains producing A_2aGH in high yields and homogeneity

Our results suggest that the use of an integrating vector enables homogenous overexpression of *A_2aGH* at levels that are otherwise unstable by episomal means. *S. cerevisiae* cells were transformed with the pITy A_2aGH vector and incubated in liquid cultures containing increasing concentrations of the corresponding selection agent. These cells were subsequently screened using fluorescence-activated cell sorting (FACS), and cells exhibiting the highest GFP fluorescence intensities were collected. Upon expression of *A_2aGH*, these cells exhibit a homogenous population with MFI values 110 – 140-fold over background and 2.5 – 3-fold greater than that of cells isolated through selection using standard plate-based protocols (pITy (500)) (**Figure 4**). Despite the marked increase in protein yields, the isolated strains consist of highly homogenous populations. Greater than 91% of all strains screened for high A_2aGH production display MFI values above background (**Figure 4B and S3**). Previous work demonstrated enhanced yields of soluble and secreted proteins in *S. cerevisiae* upon increasing integrated gene copy number, or gene dosage[34,50]. Similarly, previous studies obtained high yields of A_2aGH using the pITy A_2aGH vector through manual screening of *S. cerevisiae* transformants for those exhibiting high fluorescence intensities[51,52]. However, these

methods were extremely work- and time-intensive; thus, we developed a rapid protocol for isolating strains producing high yields of A_2aGH.

Although translational or post-translational bottlenecks have been suggested to limit production of membrane proteins like A_2aGH at high titers in *S. cerevisiae*[52], the effects of gene dosage on A_2aGH production have not been rigorously examined. To address this gap in knowledge, we quantified relative *A_2aGH* genome integration frequencies in yeast strains isolated through conventional methods (pITy (500), selected on 500 μg/mL G418) and those presented here (pITy (800 – 2400), selected on 800 - 2400 μg/mL G418). Quantitative PCR reveals a nearly linear relationship between copy number and cellular MFI for low integration frequencies as a 3.8-fold increase in *A_2aGH* copy number generates a 2.4-fold increase in MFI **(Figure 5)**. This strong relationship suggests a transcriptional bottleneck for protein production in this regime. As copy number increases further, cellular MFI increases at a non-linear rate as 5.2- and 15.3-fold increases in gene copy number result in only 2.5- and 3-fold increases in MFI, respectively. Here, A_2aGH production is likely limited by translational or post-translational bottlenecks as previously discussed. The positive relationship between gene dosage and protein yield is promising, and we expect that our method can be applied to modulate yields of well-expressing membrane proteins over a wide range by tuning gene integration frequency.

High gene dosage results in significantly improved functional A_2aGH yield

While cellular fluorescence intensity can be used to approximate total membrane protein yields, this metric does not necessarily report the amount of functional protein localized to the plasma membrane, which is critical for an engineered microbial biosensor. Here, relative yields of ligand-binding, plasma membrane-localized A_2aGH were determined using a fluorescent ligand binding assay developed in this study. Significantly, strains harboring highly integrated *A_2aGH* cassettes

(pITy (800 – 2400)) exhibit demonstrably increased specific binding of fluorescent ligand relative to all other strains (**Figure 6**). In contrast, pITy (500) exhibits binding slightly above background. Although pITy (500) exhibits MFI values 2.5 – 3-fold less than those of the highly-integrated strains, the specific signal upon incubation with 1 μM fluorescent ligand represents a ~9-fold difference. This disparity may be indicative of functional concentration-dependence; GPCR dimerization is known to influence ligand binding affinity through allosteric interactions[53] and may be responsible for the observations made in this study. Among the strains harboring non-integrating vectors, only those carrying pYES A_2aGH demonstrate specific ligand binding due to the small fraction of cells producing high yields of protein (**Figure S1A**). As the fluorescent ligand used in this study, ABEA-X-BODIPY, was synthesized as an adenosine A1 and A3 receptor agonist[54,55], it is unsurprising that receptor saturation was not reached. Our results underscore the importance of determining cellular homogeneity to optimize functional membrane protein production. For example, without this knowledge the poor yields due to the heterogeneity associated with expression from pYES may be falsely attributed to a protein or host with inherently low yields. This hypothesis could lead to cumbersome efforts such as protein engineering or screening expression conditions as opposed to the simple exchange of vector backbones.

Full-length, functional A_2aGH is produced at the yeast plasma membrane

In *S. cerevisiae*, improperly folded membrane proteins are retained in the endoplasmic reticulum (ER) or targeted to cytoplasmic proteasomes[56]. Accordingly, confocal microscopy was used to determine A_2aGH localization and provide insight on the quality of A_2aGH folding. In all strains, A_2aGH is properly targeted to the plasma membrane in addition to intracellular organelles as observed in previous reports[57] (**Figure 7**). Observations of phenotypic heterogeneity made using flow cytometry are corroborated by the micrographs for each strain. Among the yeast populations expressing *A_2aGH* from pYC or pYES vectors only a subset display GFP fluorescence intensities

above background. In contrast, all yeast cells harboring pYES-KanMX or pITy vectors exhibit detectable levels of GFP-tagged protein. Likewise, the relative GFP fluorescence intensities across strains reflect the high A_2aGH yields ascertained for strains harboring integrating vectors compared to the low yields associated with non-integrating vectors. Confocal microscopy also reveals fluorescent ligand binding at the periphery of cells with high *A_2aGH* gene dosage supporting our interpretation of fluorescent signal as specific binding as opposed to non-specific interactions such as internalization of the ligand. Slight differences in fluorescent ligand binding are apparent in these strains; however, as these are qualitative measurements for a small subset of cells, these differences do not necessarily reflect significant changes in functional protein yield.

Despite the use of a vacuolar protease deficient yeast strain[58], A_2aGH proteolysis may still occur through the myriad proteases in *S. cerevisiae*[59], which could impact receptor function. To assess the integrity of A_2aGH across the strains examined in this study, SDS-PAGE and western blotting were performed to verify production of full-length protein. In-gel fluorescence of yeast lysate reveals 3 distinct bands for each sample likely corresponding to full-length A_2aGH (~50 kDa), a cleaved C-terminal A_2aGH product (~35 kDa)[51], and a species with molecular weight similar to GFP (~27 kDa) (**Figure 8A**). The intensities of these bands are much greater for the strains harboring pITy A_2aGH reflecting increased yields of the protein. A fourth band with high molecular weight is present for the pITy-carrying strains and may correspond to a higher order oligomer species[60]. Although the expected molecular weight of A_2aGH is ~72 kDa, membrane proteins are known to deviate from expectation due to non-uniform interaction with SDS[61]. Additionally, the disulfide bonds that are formed in A_2aR may contribute to a more compact tertiary structure compounding contributions to erroneous gel migration rates[62].

In agreement with in-gel fluorescence, a subsequent anti-A_2aR western blot reveals a band of ~55 kDa for all samples corresponding to the full-length protein (**Figure 8B**). However, additional bands are visible for strains harboring integrating vectors. These samples contain a band with a molecular weight of ~63 kDa, which has been shown to correspond to the dimeric form of hA_2aR lacking a GFP tag[60]. A third band has an apparent molecular weight of ~35 kDa likely corresponding to an hA_2aR monomer lacking GFP. These data suggest that the production of primarily full-length hA_2aR is consistent across all strains. An increase in protein yields does not adversely affect protein integrity supporting the use of expression vectors as a means of improving homogeneity and yields of functional membrane proteins.

Additionally, the detection of putative hA_2aR dimers supports the hypothesis that positive allostery resulting from receptor oligomerization improves functional yields in strains with high *A_2aGH* gene dosage. The relative intensities of these 63 kDa bands are greater in strains with increased total A_2aGH yields, which matches expected behavior of equilibrium oligomerization wherein greater overall receptor yield would lead to an increase in receptor dimers. Use of GPCRs exhibiting positive allostery upon oligomerization may enable the construction of biosensors with highly improved sensitivity. Further, the large (29-fold) range in protein yield obtained in this study may be key to assaying concentration-dependent oligomerization and allostery, which are a new frontier for GPCR drug discovery[63].

In this study, we investigated the choice of expression vector as a tool to easily optimize membrane protein overexpression in *S. cerevisiae*. The data presented here demonstrate the wide, perhaps unexpected, variability in membrane protein yield and homogeneity that results from use of different classes of yeast vectors. As membrane protein overexpression is a highly complex task, we do not propose the exchange of vectors as a universal design rule to improve membrane protein

production in *S. cerevisiae*. However, we do hypothesize that the homogeneity and yield of many membrane proteins may be improved by using vectors contrary to the norm. The use of commercial, non-integrating vectors yields heterogeneous cell populations producing GPCR in low titers due to high rates of plasmid loss. These results underscore the complexity of overexpressing membrane proteins, which often leads to downstream iterative optimization efforts such as engineering and screening the protein, host, or expression conditions. However, we restore plasmid stability and cellular homogeneity by expressing the same GPCR from multi-site integrating or modified high copy vectors. This method of exchanging vectors requires far less resources compared to conventional routes of optimizing membrane protein overexpression.

Although the multi-site integrating vector enables production of GPCR in high titers, it is critical to distinguish between yields of total and functional protein particularly for applications such as GPCR-based sensors. The importance of this distinction is exemplified by our finding that strains isolated through conventional plate-based selection have low functional yields. To improve yields of functional GPCR, we developed a screening methodology to rapidly isolate highly overexpressing cells using a fluorescent tag and FACS. The FACS-isolated strains display marked improvements in functional GPCR yield without loss of homogeneity. Therefore, we propose that this method can supplement or even replace time-intensive screens for cells producing high yields of membrane proteins for structural characterization. The novel, modified high copy vector addresses the need for homogenous GPCR production without integration into the genome to facilitate applications in which plasmid recovery and subsequent analysis or mutagenesis is desired, such as in receptor engineering. Further, the homogeneity afforded by the integrating and modified vectors is essential for tight control of metabolic flux and high signal-to-noise ratios in reporter systems.

Materials and Methods

Plasmid construction

The multi-site integrating pITy-A_2aR-GFP-His_{10} (pITy A_2aGH) plasmid was previously constructed[51] and used for integrated gene expression in this study. The A_2aR-GFP-His_{10} (A_2aGH) fusion protein contains an N-terminal prepro leader sequence to aid in translocation and trafficking to the plasma membrane[64]. In the pITy vector, gene expression is under the control of a bidirectional GAL1,10 promoter. Centromeric and episomal A_2aGH vectors were constructed using the pYC2 and pYES2 vector backbones (Invitrogen), respectively. Standard polymerase chain reaction (PCR) techniques[65] were used to append flanking *HindIII* and *XhoI* restriction sites to the prepro-A_2aR-GFP-His_{10} coding sequence, which was amplified from pITy A_2aGH using primers 1 and 2. The vectors and genes were digested, ligated, and transformed into *Escherichia coli* DH5α. The pYES-KanMX-A_2aR-GFP-His_{10} construct was generated by subcloning the P_{TEF1}-KanMX-T_{TEF1} cassette from pYM39 into pYES-A_2aR-GFP-His_{10}[66]. The gene cassette was amplified using primers 3 and 4 introducing flanking *SpeI* restriction sites to the sequence. In all non-integrating vectors, the A_2aGH cassette is under the control of the galactose-inducible GAL1 promoter. All plasmids were transformed into *Saccharomyces cerevisiae* using the high efficiency lithium acetate protocol[67].

Yeast strains and culturing conditions

S. cerevisiae strain BJ5464 (MATα *ura3-52 trp1 leu2Δ1 hisΔ200 pep4::HIS3 prbΔ1.6R can1*) (ATCC) was used for all experiments described in this study. Culture maintenance and gene expression were performed in a shaker incubated at 30°C and 250 r.p.m. Strains harboring pITy A_2aGH were maintained in synthetic dextrose medium supplemented with casamino acids (SD-2XSCAA) [68]. Strains harboring centromeric or episomal plasmids were maintained in SD-2XSCAA medium lacking uracil (SD-2XSCAA –ura). Prior to *A_2aGH* or *Ste2p-GH* expression, strains were subcultured into 5 mL SR-2XSCAA or SR-2XSCAA -ura containing 2% (w/v) raffinose at an initial OD_{600} of 0.5.

Upon reaching an OD_{600} between 2 – 3, gene expression was induced by subculturing strains into 5 mL SRG-2XSCAA or SRG-2XSCAA –ura containing 2% (w/v) raffinose and 2% (w/v) galactose at an initial OD_{600} of 0.2. Gene expression was carried out for 12 hours.

Fluorescence-activated cell sorting

Fluorescence-activated cell sorting (FACS) analyses described in this report were performed using a BD FACSARIA I flow cytometer. Yeast cultures were diluted to an OD_{600} unit of 1.0 in a 1 mL volume of 1X phosphate buffered saline (PBS) prior to FACS analysis. Scatter and fluorescence intensity data were collected for approximately 60,000 singlet cells from each sample using a 488 nm laser and 530/30 nm bandpass filter. Data analysis was performed using FlowJo software.

Ligand binding assays

Yeast cells expressing *A_2aGH* were grown to an OD_{600} value between 2 – 3 and pelleted at 3000g for 30s. Cells were resuspended in binding buffer (50 mM Tris-HCl, 10 mM MgCl2, pH = 6) and incubated with the fluorescent adenosine A1 and A3 receptor agonist ABEA-X-BY630 (NIMH, Bethesda, MD) while protected from light for 1 hour at room temperature. Samples were placed on ice for 30 minutes prior to resuspension in 1X PBS (pH = 6) and analysis with FACS using a 488 nm laser and 530/30 nm bandpass filter to measure fluorescence from GFP and a 633 nm laser and 660/20 nm bandpass filter to measure fluorescence from the BODIPY fluorophore on the ligand.

Isolation of yeast strains with high *A_2aGH* gene dosage

Yeast strains harboring highly integrated P_{GAL1}-prepro-hA_2AR-GFP-His_{10} cassettes were generated by transforming cells with 10 µg pITy A_2aGH linearized using *BsaBI*. Transformed cells were allowed to recover by shaking at 30°C in 1 mL YPD for 5 hours. 100 µL of recovered cells were used to inoculate 5 mL YPD (1% yeast extract, 2% peptone, 2% dextrose) containing either 800, 1600, or

2400 μg/mL G418 and incubated at 30°C with shaking until culture turbidity had markedly increased corresponding to final OD_{600} values between 10 – 25. These cells were used to inoculate 5 mL YPG (1% yeast extract, 2% peptone, 2% galactose) cultures at an initial OD_{600} of 0.2 in order to induce A_2aGH expression. Cells were prepared for FACS analysis and sorting as described above, and 100,000 cells displaying the highest fluorescence intensities were sorted into 5 mL YPD containing 500 μg/mL G418 and incubated overnight with at 30°C with shaking.

Quantitative PCR

Determination of relative plasmid copy number and *A_2aGH* integration frequencies was carried out using quantitative PCR (qPCR). Yeast strains expressing *A_2aGH* were grown to an OD_{600} value between 2 – 4 prior to total DNA extraction[69]. Extracted DNA concentrations were used as templates for qPCR using BioRad iQ5 and SsoAdvanced Universal SYBR Green Supermix. A region within the *hA_2aR* gene was amplified using primers 5' AAAGGAGGGCAAGAACCACT 3' and 5' TAGACACCCAGCATGAGCAG 3'. *A_2aGH* copy numbers were normalized to the copy number of a single copy genomic target, *Ssn6*, amplified using primers 5' TGCAGCAAAGGGAGTTTCT 3' and 5' GCGGATGTTCCATAGCTTGT 3'. All qPCR experiments were performed with three biological replicates in technical duplicate.

Plasmid loss assay

The extent of plasmid loss within engineered yeast strains were determined by counting the number of colony forming units (CFU) that emerged on selective and non-selective media. Yeast strains were cultured as described above. Prior to subculturing strains into raffinose-containing media, cultures were serially diluted and plated onto both SD-2XSCAA and SD-2XSCAA -ura plates. Gene expression was induced in yeast strains, and cells were serially diluted and plated onto SD-2XSCAA and SD-2XSCAA -ura in the same manner.

SDS-PAGE, in-gel fluorescence, and western blotting

A_2aGH expression was induced as described above. Yeast lysate was prepared for SDS-PAGE as described previously[60] with few modifications. Briefly, cells equivalent to 2.5 OD_{600} units were pelleted at 6000g for 30s and resuspended in 25 µL YPER (Thermo Scientific). Samples were incubated at room temperature for 30 minutes prior to incubation with an equal volume of 2X Laemmli buffer (4% (w/v) SDS, 20% (v/v) glycerol, 125 mM Tris-HCl pH 6.8, 100 mM dithiothreitol, 0.01% Bromophenol blue) at 37°C for 1 hour. Cell debris was pelleted at 6000g for 30s, and 20 µL sample volumes were loaded into each lane of a 10% Tris-Glycine gel. Precision Plus Protein WesternC (BioRad) and MagicMark XP (Invitrogen) molecular weight ladders were used at standards. In-gel fluorescence due to GFP was imaged using Blue Epi illumination and a 530/28 nm bandpass filter. Following imaging of in-gel fluorescence, proteins were transferred to nitrocellulose membranes and probed with primary anti-A_2a antibody (sc32261, Santa Cruz Biotechnology, Paso Robles, CA) and secondary DyLight 550 antibody (ab96880, Abcam, Cambridge, MA) as described previously[60].

Confocal Microscopy

A_2aGH expression and fluorescent ligand binding were performed as described above. Following resuspension of samples to 0.1 OD_{600} units in 1X PBS, cells were transferred to Nunc Lab-Tek chambered slides coated with 0.1% (w/v) poly-L-lysine (Sigma-Aldrich). Microscopy was performed using an Olympus Fluoview 1000 Spectral confocal microscope with a 60x/NA 1.3 objective.

Acknowledgements

We thank Professor Patrick Daugherty (Department of Chemical Engineering, University of California, Santa Barbara) for pYC2, Dr. Westermann (Universität Bayreuth, Germany) for pYES2, Professor Anne Robinson (Department of Chemical Engineering, Tulane University) for pITy. The fluorescent ligand ABEA-X-BY630 was generously provided by the NIMH Chemical Synthesis and Drug Supply Program. We acknowledge the use of the NRI-MCDB microscopy facility supported by NIH award No. S10OD010610-01A1. We acknowledge funding support from a Hellman Faculty Fellowship awarded to MAO, and the University of California Cancer Research Coordinating Committee. JIY acknowledges support from a National Science Foundation Graduate Research Fellowship under grant No. 1650114.

Supplemental Information

Supplemental information to support this manuscript are available online. This information details construction and evaluation of the tTA-KanMX A_2aGH tunable expression plasmid, as well as expression of STE2p in different vector systems in yeast. Primer sequences, qPCR data, and supplementary FACS plots of A_2aGH expression under different vector conditions are located in the supplement.

Author Information

JIY and MAO designed experiments, analyzed data, and wrote the manuscript. JIY performed all experiments detailed in the manuscript.

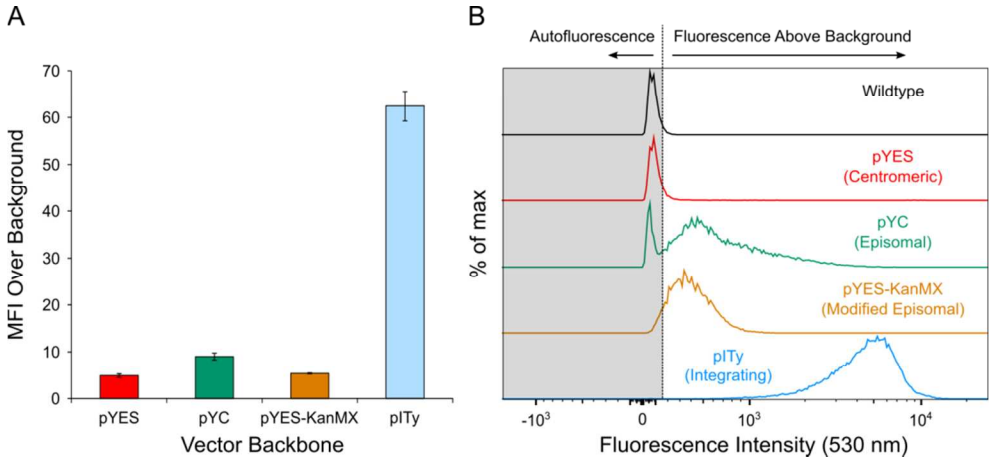

Figure 1: Flow cytometric analysis of *A_2aGH* expression from various yeast vectors results in a range of total protein yields and cellular homogeneities. (A) Yeast strains expressing *A_2aGH* from non-integrating (pYES, pYC, pYES-KanMX) vectors exhibit 5 – 9-fold increases in cellular mean fluorescence intensity (MFI) values relative to background autofluorescence. In contrast, the use of a multi-site integrating (pITy) vector results in a 62-fold improvement in MFI over background. (B) A significant number of cells within populations expressing *A_2aGH* from commercial, non-integrating vectors display fluorescence intensities comparable to a wildtype control lacking an *A_2aGH* vector. Homogeneity is restored upon gene expression in a novel, modified episomal (pYES-KanMX) vector or multi-site integrating vector. In panel A, data represent the mean of three biological replicates, and error bars represent their standard deviation. In panel B, each histogram corresponds to a representative sample.

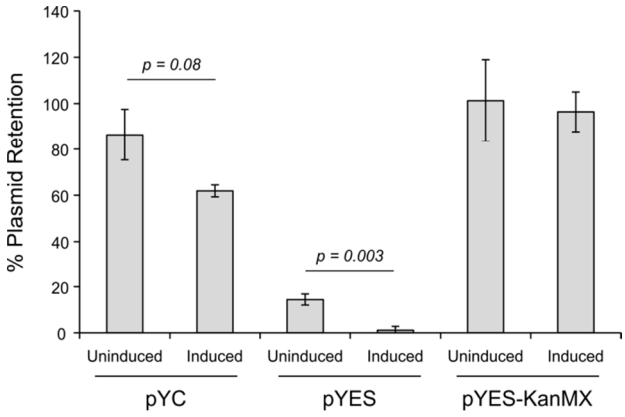

Figure 2: Determination of colony forming units (CFU) grown on permissive and selective media enables quantification of non-integrating plasmid loss. Plasmid retention % represents CFU formed on media lacking the corresponding auxotrophic marker (selective) relative to those formed on media containing the marker (permissive). CFU values were measured prior to (uninduced) and during (induced) A_2aGH expression from non-integrating vectors. Data represent the mean of three biological replicates, and error bars represent their standard deviation. Statistical significance was determined through calculation of *p* values using a paired Student's t-test.

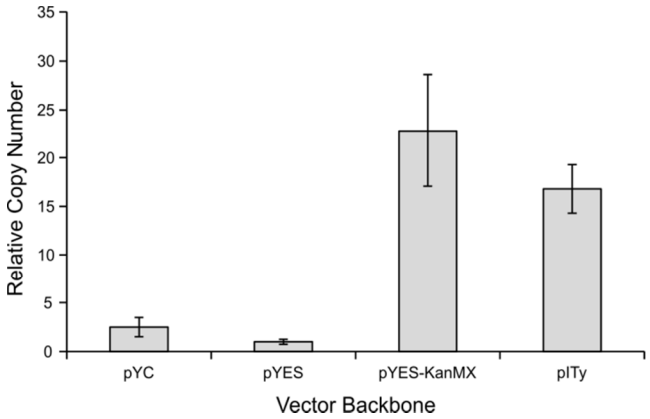

Figure 3: Determination of relative vector copy numbers using quantitative PCR suggests varying mitotic stabilities are observed for each vector. After induction of *A_2aGH* expression, the average copy number of the low copy pYC A_2aGH vector is 2.5-fold greater than the high copy pYES A_2aGH vector, suggesting significant pYES plasmid loss. Surprisingly, the relative copy number of the pYES-KanMX A_2aGH vector is 22.8-fold greater than that of the pYES A_2aGH vector and 1.4-fold greater than the copy number of the integrated pITy A_2aGH cassette. Data represent the mean of three biological replicates, and error bars represent their standard deviation.

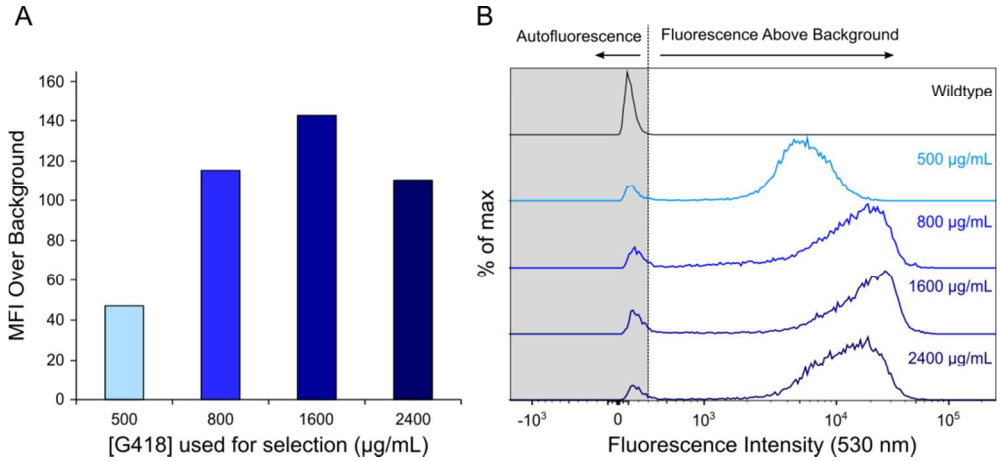

Figure 4: Flow cytometric analysis of GPCR expression demonstrates increasing gene dosage and elevated protein yields without loss of homogeneity. (A) Yeast strains were transformed with a multi-site integrating vector containing the *A_2aGH* cassette and used to inoculate liquid media containing increasing concentrations (800, 1600, and 2400 μg/mL) of the corresponding chemical selection agent (G418). Within these populations, cells exhibiting the greatest MFI values were sorted and compared to a strain selected from plates using 500 μg/mL G418. Strains sorted in liquid media display a 2.5 – 3-fold increase in cellular MFI relative to a strain selected from plates. (B) Despite increased A_2aGH yields, all strains display high degrees of homogeneity. In each population, the majority of cells display high fluorescence intensities while only few cells exhibit fluorescence intensities comparable to a wildtype negative control. In panel A, data represent the mean of ~20,000 measurements of single cells. In panel B, each histogram corresponds to a representative sample.

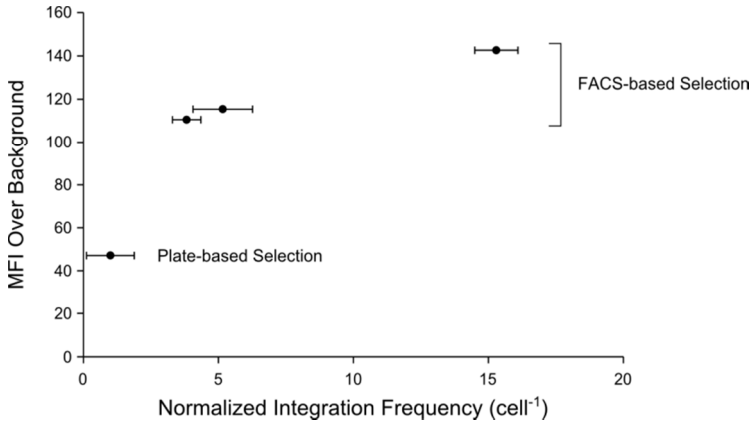

Figure 5: Quantitative PCR reveals a non-linear relationship between total protein yield and GPCR genomic integration frequency. Average integration frequencies were determined for yeast strains isolated using conventional plate-based selection (pITy (500)) and through our FACS approach (pITy (800 - 2400)). Flow cytometry was used to measure the cellular MFI for approximately 20,000 single cells for each strain. Data represent the mean of three biological replicates, and error bars represent their standard deviation.

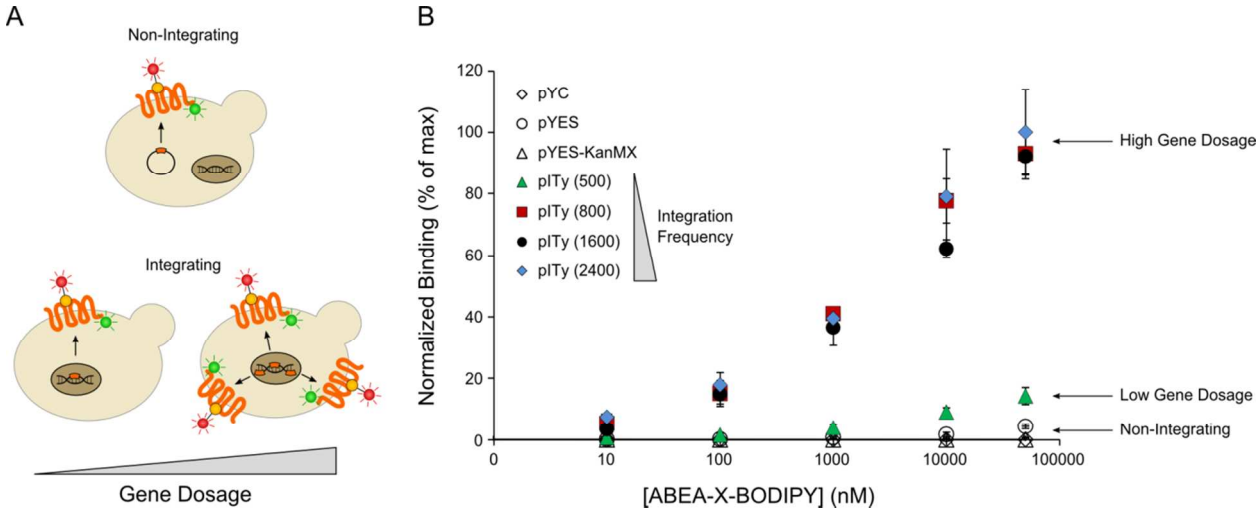

Figure 6: Fluorescent ligand binding verifies that elevated total protein yields also bolster yields of functional, plasma membrane-localized receptor. (A) A red fluorescent adenosine receptor agonist binds specifically to functional A_2aGH at the periphery of the cell enabling quantification of functional protein localized to the plasma membrane. (B) Yeast strains producing A_2aGH from non-integrating or integrating vectors were incubated with varying concentrations of a red fluorescent A1/A3 adenosine receptor agonist, ABEA-X-BODIPY, and analyzed using flow cytometry. Strains sorted for high gene dosage exhibit relatively high yields of functional, membrane-localized A_2aGH compared to strains with low gene dosage or expressing *A_2aGH* from non-integrating vectors. For each ligand concentration, specific binding was calculated by subtracting background signal from the signal measured for each sample. Background signal was measured for each ligand concentration using a wildtype negative control. All data was normalized to the maximum signal measured across all samples. Data represent the mean of three biological replicates, and error bars represent their standard deviation.

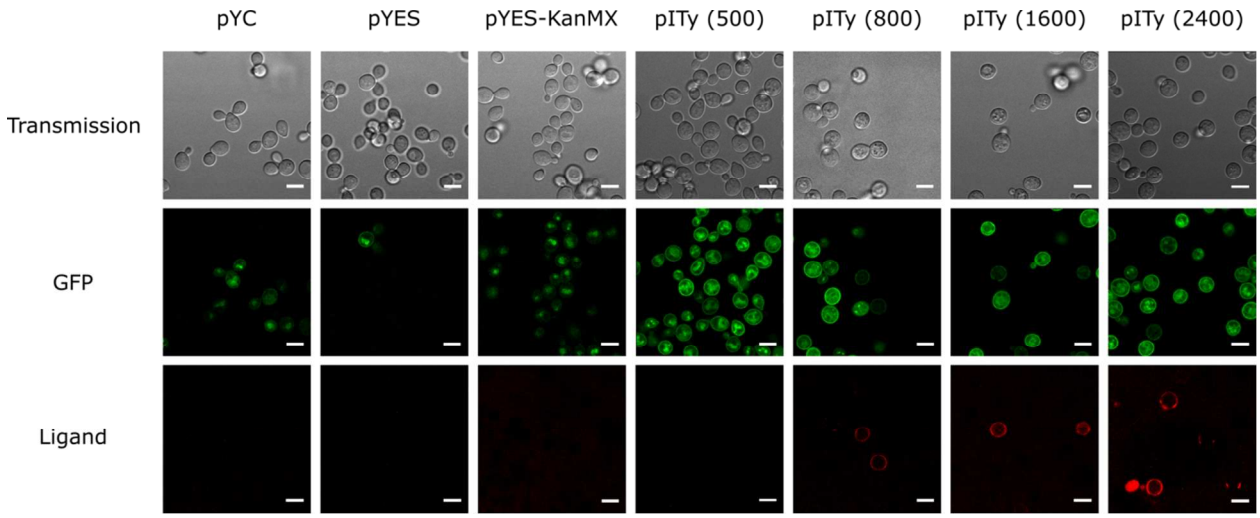

Figure 7: Representative confocal micrographs of yeast strains producing A_2aGH from various vectors demonstrate variable protein yield, homogeneity, and binding of fluorescent ligand. The use of a GFP-tag also enables visualization of A_2aGH trafficking, which is directed to the plasma membrane and endoplasmic reticulum in all strains. Transmission and GFP micrographs were captured for strains harboring different yeast vectors after overnight induction of *A_2aGH* expression in raffinose- and galactose-based medium. Micrographs depicting binding of fluorescent ligand (Ligand) were captured after incubation of cells with 1 µM fluorescent A1/A3 adenosine receptor agonist, AXB. Microscopy was performed using an Olympus Fluoview 1000 Spectral confocal microscope equipped with a 60x/NA 1.3 objective. All scale bars represent 5 µm.

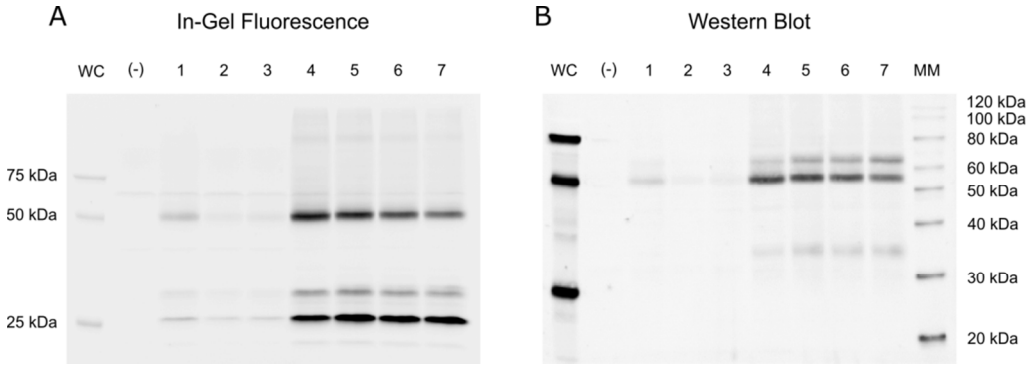

Figure 8: Analysis of A_2aGH integrity reveals two predominant species of full-length, monomeric A_2aGH and a putative hA_2aR dimer lacking GFP. (A) In-gel fluorescence identifies protein species containing properly folded GFP. (B) Western blot of the same gel using an anti-A_2aR antibody binding to the third intracellular loop identifies protein species containing the targeted epitope. In both gels lanes represent WC – WesternC standard, MM – MagicMark standard, (-) – wildtype negative control, and strains harboring 1 – pYC A_2aGH, 2 – pYES A_2aGH, 3 – pYES-KanMX A_2aGH, 4 – pITy (500), 5 – pITy (800), 6 – pITy (1600), 7 – pITy (2400).

References

1. Kell, D. B., Swainston, N., Pir, P. & Oliver, S. G. Membrane transporter engineering in industrial biotechnology and whole cell biocatalysis. *Trends Biotechnol.* **33,** 237–246 (2015).

2. Bill, R. M. *et al.* Overcoming barriers to membrane protein structure determination. *Nat. Biotechnol.* **29,** 335–340 (2011).

3. Adeniran, A., Sherer, M. & Tyo, K. E. J. Yeast-based biosensors: Design and applications. *FEMS Yeast Res.* **15,** 1–15 (2015).

4. Rogers, J. K., Taylor, N. D. & Church, G. M. Biosensor-based engineering of biosynthetic pathways. *Curr. Opin. Biotechnol.* **42,** 84–91 (2016).

5. Mukherjee, K., Bhattacharyya, S. & Peralta-Yahya, P. GPCR-Based Chemical Biosensors for Medium-Chain Fatty Acids. *ACS Synth. Biol.* **4,** 1261–1269 (2015).

6. Radhika, V. *et al.* Chemical sensing of DNT by engineered olfactory yeast strain. *Nat. Chem. Biol.* **3,** 325–330 (2007).

7. Ehrenworth, A. M., Claiborne, T. & Peralta-Yahya, P. Medium-Throughput Screen of Microbially Produced Serotonin via a G-Protein-Coupled Receptor-Based Sensor. *Biochemistry* **56,** 5471–5475 (2017).

8. Nakamura, Y., Ishii, J. & Kondo, A. Applications of yeast-based signaling sensor for characterization of antagonist and analysis of site-directed mutants of the human serotonin 1A receptor. *Biotechnol. Bioeng.* **112,** 1906–1915 (2015).

9. Ault, A. D. & Broach, J. R. Creation of GPCR-based chemical sensors by directed evolution in yeast. *Protein Eng. Des. Sel.* **19,** 1–8 (2006).

10. Kinzer-Ursem, T. L. & Linderman, J. J. Both ligand- and cell-specific parameters control ligand

agonism in a kinetic model of G protein-coupled receptor signaling. *PLoS Comput. Biol.* **3,** 0084–0094 (2007).

11. Hauser, A. S., Misty, A., Mathias, R.-A., Schiöth, H. B. & Gloriam, D. E. Trends in GPCR drug discovery: new agents, targets and indications. *Nat. Rev. Drug Discov.* (2017). doi:10.1038/nrd.2017.178

12. Jazayeri, A., Dias, J. M. & Marshall, F. H. From G protein-coupled receptor structure resolution to rational drug design. *J. Biol. Chem.* **290,** 19489–19495 (2015).

13. Freigassner, M., Pichler, H. & Glieder, A. Tuning microbial hosts for membrane protein production. *Microb. Cell Fact.* **8,** 69 (2009).

14. Lee, M. E., DeLoache, W. C., Cervantes, B. & Dueber, J. E. A Highly Characterized Yeast Toolkit for Modular, Multipart Assembly. *ACS Synth. Biol.* **4,** 975–986 (2015).

15. Jensen, N. B. *et al.* EasyClone: Method for iterative chromosomal integration of multiple genes in Saccharomyces cerevisiae. *FEMS Yeast Res.* **14,** 238–248 (2014).

16. Ma, J. *et al.* Structure of rat monoamine oxidase A and its specific recognitions for substrates and inhibitors. *J. Mol. Biol.* **338,** 103–114 (2004).

17. Son, S.-Y. *et al.* Structure of human monoamine oxidase A at 2.2-A resolution: The control of opening the entry for substrates/inhibitors. *Proc. Natl. Acad. Sci.* **105,** 5739–5744 (2008).

18. Pedersen, B. P. *et al.* Crystal structure of a eukaryotic phosphate transporter. *Nature* **496,** 533–536 (2013).

19. Parker, J. L. & Newstead, S. Molecular basis of nitrate uptake by the plant nitrate transporter NRT1.1. *Nature* **507,** 68–72 (2014).

20. Lin, S.-M. *et al.* Crystal structure of a membrane-embedded H+-translocating pyrophosphatase.

Nature **484,** 399–403 (2012).

21. Kellosalo, J., Kajander, T., Kogan, K., Pokharel, K. & Goldman, A. The Structure and Catalytic Cycle of a Sodium-Pumping Pyrophosphatase. *Science (80-.).* **337,** 473–476 (2012).

22. Brunner, J. D., Lim, N. K., Schenck, S., Duerst, A. & Dutzler, R. X-ray structure of a calcium-activated TMEM16 lipid scramblase. *Nature* **516,** 207–212 (2014).

23. Kintzer, A. F. & Stroud, R. M. Structure, inhibition and regulation of two-pore channel TPC1 from Arabidopsis thaliana. *Nature* **531,** 258–264 (2016).

24. Huynh, K. W. *et al.* Structure of the full-length TRPV2 channel by cryo-EM. *Nat. Commun.* **7,** 11130 (2016).

25. van den Berg, B. *et al.* Structural basis for Mep2 ammonium transceptor activation by phosphorylation. *Nat. Commun.* **7,** 11337 (2016).

26. Kapoor, K. *et al.* Mechanism of inhibition of human glucose transporter GLUT1 is conserved between cytochalasin B and phenylalanine amides. *Proc. Natl. Acad. Sci.* **113,** 4711–4716 (2016).

27. Alguel, Y. *et al.* Structure of eukaryotic purine/H+ symporter UapA suggests a role for homodimerization in transport activity. *Nat. Commun.* **7,** 11336 (2016).

28. Li, K.-M. *et al.* Membrane pyrophosphatases from Thermotoga maritima and Vigna radiata suggest a conserved coupling mechanism. *Nat. Commun.* **7,** 13596 (2016).

29. Clausen, J. D. *et al.* SERCA mutant E309Q binds two Ca 2+ ions but adopts a catalytically incompetent conformation. *EMBO J.* **32,** 3231–3243 (2013).

30. Pryor, E. E. *et al.* Structure of the Integral Membrane Protein CAAX Protease Ste24p. *Science (80-.).* **339,** 1600–1604 (2013).

31. Wittrup, K. D., Robinson, A. S., Parekh, R. N. & Forrester, K. J. Existence of an Optimum Expression Level for Secretion of Foreign Proteins in Yeast. *Ann. N. Y. Acad. Sci.* **745,** 321–330 (1994).

32. Clarke, L. & Carbon, J. Isolation of a yeast centromere and construction of functional small circular chromosomes. *Nature* **287,** 504–509 (1980).

33. Gnügge, R., Liphardt, T. & Rudolf, F. A shuttle vector series for precise genetic engineering of Saccharomyces cerevisiae. *Yeast* **33,** 83–98 (2016).

34. Parekh, R. N., Shaw, M. R. & Wittrup, K. D. An integrating vector for tunable, high copy, stable integration into the dispersed Ty delta sites of Saccharomyces cerevisiae. *Biotechnol. Prog.* **12,** 16–21 (1996).

35. Romanos, M. A., Scorer, C. A. & Clare, J. J. Foreign gene expression in yeast: a review. *Yeast* **8,** 423–488 (1992).

36. Newstead, S., Kim, H., von Heijne, G., Iwata, S. & Drew, D. High-throughput fluorescent-based optimization of eukaryotic membrane protein overexpression and purification in Saccharomyces cerevisiae. *Proc. Natl. Acad. Sci. U. S. A.* **104,** 13936–13941 (2007).

37. Hegemann, J. H. *et al.* A fast method to diagnose chromosome and plasmid loss in Saccharomyces cerevisiae strains. *Yeast* **15,** 1009–19 (1999).

38. Parekh, R., Forrester, K. & Wittrup, D. Multicopy Overexpression of Bovine Pancreatic Trypsin Inhibitor Saturates the Protein Folding and Secretory Capacity of Saccharomyces cerevisiae. *Protein Expr. Purif.* **6,** 537–545 (1995).

39. Li, M. *et al.* Selecting Optimum Eukaryotic Integral Membrane Proteins for Structure Determination by Rapid Expression and Solubilization Screening. *J. Mol. Biol.* **385,** 820–830

(2009).

40. Shiroishi, M. *et al.* Platform for the rapid construction and evaluation of GPCRs for crystallography in Saccharomyces cerevisiae. *Microb. Cell Fact.* **11,** 78 (2012).

41. Shiroishi, M., Moriya, M. & Ueda, T. Micro-scale and rapid expression screening of highly expressed and/or stable membrane protein variants in Saccharomyces cerevisiae. *Protein Sci.* **25,** 1863–1872 (2016).

42. Byrne, B. Pichia pastoris as an expression host for membrane protein structural biology. *Curr. Opin. Struct. Biol.* **32,** 9–17 (2015).

43. Sarwar, M. & Akhtar, M. Cloning of aminoglycoside phosphotransferase (APH) gene from antibiotic-producing strain of Bacillus circulans into a high-expression vector, pKK223-3. Purification, properties and location of the enzyme. *Biochem. J.* **268,** 671–7 (1990).

44. Ozbudak, E. M., Thattai, M., Kurtser, I., Grossman, A. D. & van Oudenaarden, A. Regulation of noise in the expression of a single gene. *Nat. Genet.* **31,** 69–73 (2002).

45. Garí, E., Piedrafita, L., Aldea, M. & Herrero, E. A set of vectors with a tetracycline-regulatable promoter system for modulated gene expression in Saccharomyces cervisiae. *Yeast* **13,** 837–848 (1997).

46. Adeniran, A., Stainbrook, S., Bostick, J. W. & Tyo, K. E. J. Detection of a Peptide Biomarker by Engineered Yeast Receptors. *ACS Synth. Biol.* **7,** 696–705 (2018).

47. Di Roberto, R. B., Chang, B., Trusina, A. & Peisajovich, S. G. Evolution of a G protein-coupled receptor response by mutations in regulatory network interactions. *Nat. Commun.* **7,** 12344 (2016).

48. Stainbrook, S. C., Yu, J. S., Reddick, M. P., Bagheri, N. & Tyo, K. E. J. Modulating and evaluating receptor promiscuity through directed evolution and modeling. *Protein Eng. Des. Sel.*

1–11 (2017). doi:10.1093/protein/gzx018

49. Fukuda, N., Kaishima, M., Ishii, J. & Honda, S. Positive Detection of GPCR Antagonists Using a System for Inverted Expression of a Fluorescent Reporter Gene. *ACS Synth. Biol.* acssynbio.7b00056 (2017). doi:10.1021/acssynbio.7b00056

50. Lee, F. W. & Da Silva, N. a. Sequential delta-integration for the regulated insertion of cloned genes in Saccharomyces cerevisiae. *Biotechnol. Prog.* **13,** 368–373 (1997).

51. O'Malley, M. A., Lazarova, T., Britton, Z. T. & Robinson, A. S. High-level expression in Saccharomyces cerevisiae enables isolation and spectroscopic characterization of functional human adenosine A2a receptor. *J. Struct. Biol.* **159,** 166–78 (2007).

52. Niebauer, R. T., Wedekind, A. & Robinson, A. S. Decreases in yeast expression yields of the human adenosine A2a receptor are a result of translational or post-translational events. *Protein Expr. Purif.* **37,** 134–143 (2004).

53. Ferré, S. *et al.* G protein-coupled receptor oligomerization revisited: functional and pharmacological perspectives. *Pharmacol. Rev.* **66,** 413–34 (2014).

54. Cordeaux, Y., Briddon, S. J., Alexander, S. P. H., Kellam, B. & Hill, S. J. Agonist-occupied A3 adenosine receptors exist within heterogeneous complexes in membrane microdomains of individual living cells. *FASEB J.* **22,** 850–860 (2007).

55. Middleton, R. J. *et al.* New fluorescent adenosine A1-receptor agonists that allow quantification of ligand-receptor interactions in microdomains of single living cells. *J. Med. Chem.* **50,** 782–793 (2007).

56. Delic, M. *et al.* The secretory pathway: Exploring yeast diversity. *FEMS Microbiol. Rev.* **37,** 872–914 (2013).

57. O'Malley, M. A. *et al.* Progress toward heterologous expression of active G-protein-coupled receptors in Saccharomyces cerevisiae: Linking cellular stress response with translocation and trafficking. *Protein Sci.* **18,** 2356–70 (2009).

58. Jones, E. W. Tackling the Protease Problem in Saccharomyces cerevisiae. *Method Enzymol.* **194,** 428–53 (1991).

59. Jones, E. W. The Synthesis and Function of Proteases in Saccharomyces: Genetic Approaches. *Annu. Rev. Genet.* **18,** 233–270 (1984).

60. Schonenbach, N. S., Rieth, M. D., Han, S. & O'Malley, M. A. Adenosine A2a receptors form distinct oligomers in protein detergent complexes. *FEBS Lett.* **590,** 3295–3306 (2016).

61. Rath, A., Glibowicka, M., Nadeau, V. G., Chen, G. & Deber, C. M. Detergent binding explains anomalous SDS-PAGE migration of membrane proteins. *Proc. Natl. Acad. Sci. U. S. A.* **106,** 1760–5 (2009).

62. Pitt-Rivers, R. & Impiombato, F. S. The binding of sodium dodecyl sulphate to various proteins. *Biochem. J.* **109,** 825–830 (1968).

63. Wootten, D., Christopoulos, A. & Sexton, P. M. Emerging paradigms in GPCR allostery: implications for drug discovery. *Nat. Rev. Drug Discov.* **12,** 630–44 (2013).

64. Clements, J. M., Catlin, G. H., Price, M. J. & Edwards, R. M. Secretion of human epidermal growth factor from Saccharomyces cerevisiae using synthetic leader sequences. *Gene* **106,** 267–271 (1991).

65. Erlich, A., Gelfand, D. & Sninsky, J. J. Recent Advances in the Polymerase Chain Reaction. *Science (80-.).* **252,** 1643–1651 (1991).

66. Janke, C. *et al.* A versatile toolbox for PCR-based tagging of yeast genes: New fluorescent

proteins, more markers and promoter substitution cassettes. *Yeast* **21,** 947–962 (2004).

67. Gietz, R. D. & Woods, R. A. Transformation of Yeast by Lithium Acetate/Single-Stranded Carrier DNA/Polyethylene Glycol Method. *Methods Enzymol.* **350,** 87–96 (2002).

68. Wittrup, K. D. & Benig, V. Optimization of amino acid supplements for heterologous protein secretion in Saccharomyces cerevisiae. *Biotechnol. Tech.* **8,** 161–166 (1994).

69. Löoke, M., Kristjuahan, K. & Kristjuhan, A. Extraction of Genomic Dna From Yeasts for Pcr-Based Applications. *Biotechniques* **50,** 325–328 (2011).